

# Low mass diffractive systems at LHC

R. Schicker<sup>1</sup>,

<sup>1</sup> *Phys.Inst., Philosophenweg 12, 69120 Heidelberg*

August 30, 2021

## Abstract

Diffractive reactions in proton-proton collisions are characterized by the presence of rapidity gaps and by forward scattered protons. A diffractive trigger can therefore be defined by the tagging of the forward proton or by the detection of rapidity gaps. I present a diffractive trigger scheme for the ALICE detector at the large hadron collider LHC and discuss some physics topics. In particular, I concentrate on the low mass sector in central exclusive diffraction which becomes accessible by a double gap trigger.

## 1 The ALICE detector

The ALICE experiment at the LHC is designed as a general purpose experiment with a central barrel covering the pseudorapidity range  $-0.9 < \eta < 0.9$  and a muon spectrometer covering the range  $-4.0 < \eta < -2.5$  [1, 2]. The ALICE experimental program foresees data taking in pp and PbPb collisions at luminosities of  $\mathcal{L} = 5 \times 10^{30} \text{cm}^{-2} \text{s}^{-1}$  and  $\mathcal{L} = 10^{27} \text{cm}^{-2} \text{s}^{-1}$ , respectively. An asymmetric system pPb will be measured at a luminosity of  $\mathcal{L} = 10^{29} \text{cm}^{-2} \text{s}^{-1}$ .

The central detectors track and identify particles from  $\sim 100 \text{ MeVc}^{-1}$  to  $\sim 100 \text{ GeVc}^{-1}$  transverse momenta. Short-lived particles such as hyperons, D and B mesons are identified by their reconstructed secondary decay vertex. The detector granularity is chosen such that these tasks can be performed in a high multiplicity environment of up to 8000 charged particles per unit of rapidity. Tracking of particles is achieved by the inner tracking system (ITS) of two layers of silicon pixel (SPD), two layers of silicon strip (SSD) and two layers of silicon drift detectors (SDD). The global reconstruction of particle momentum uses the ITS information together with the information from a large Time-Projection-Chamber (TPC) and a high granularity Transition-Radiation Detector (TRD). Particle identification in the central barrel is performed by measuring energy loss in the tracking detectors, transition radiation in the TRD and time-of-flight in a high-resolution TOF array. A single arm High-Momentum Particle Identification Detector (HMPID) with limited solid angle coverage extends the momentum range of identified hadrons. Photons will be measured by a crystal  $\text{PbWO}_4$  PHOTon Spectrometer (PHOS) and an electromagnetic sampling calorimeter (EMCAL).

Additional detectors for trigger purposes and for event classification are placed on both sides of the central barrel such that the pseudorapidity range  $-3.7 < \eta < 5$  is covered. Fig. 1 shows the pseudorapidity acceptance of ALICE resulting from the ALICE detectors as explained above. The event characterization detectors shown in this figure are quartz

scintillation detectors (T0A,T0C) used for timing, plastic scintillator detectors (V0A,V0C) and silicon detectors (FMD) for multiplicity characterization.

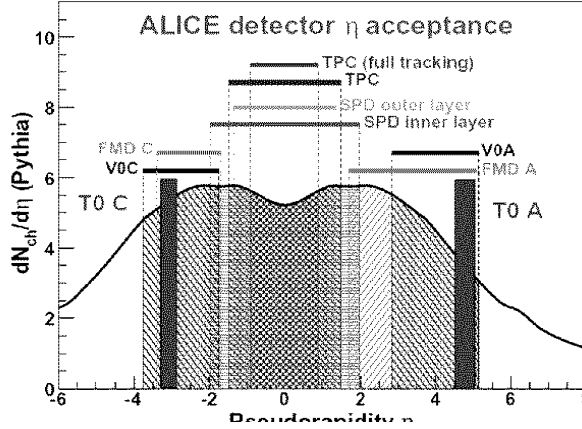


Figure 1: Pseudorapidity coverage of the different detector systems of ALICE

At very forward angles, a neutron calorimeter is placed on both sides of ALICE at a distance of 116 m from the interaction point[3]. The LHC dipoles which are located between this detector and the interaction point deflect the charged particles such that only neutral particles emitted at  $0^0$  reach this detector.

## 1.1 The diffractive gap trigger in ALICE

The ALICE trigger is designed as a system with three levels L0,L1,L2 and a high-level software trigger (HLT). A diffractive L0 trigger can be defined by requiring little or no activity in the V0A and V0C detectors explained above. These two detectors are designed with an eight and four-fold segmentation in azimuth and pseudorapidity, respectively. The segmentation in pseudorapidity allows to select a gap width in steps of half a unit up to the maximum pseudorapidity interval of two covered by the detectors.

The high-level trigger has access to the information of all the detectors shown in Fig. 1 and hence can increase the rapidity gap to the range  $-3.7 < \eta < -0.9$  and  $0.9 < \eta < 5.0$ , respectively.

Due to the absence of a V0A and V0C signal in a diffractive trigger, the L0 signal for this trigger has to be defined within the central barrel. In defining a L0 diffractive trigger, the transition radiation detector needs special consideration. This detector system is put in sleep mode after readout of an event in order to reduce power consumption. A wakeup signal is necessary to activate the onboard readout electronics. The V0A and V0C signals are transferred to the TRD pretrigger system where such a wakeup signal is generated.

A L0 diffractive trigger can, for example, be defined by the silicon pixel detector of the inner tracking system. This signal is, however, not in time for the wakeup call of the transition radiation detector. A TRD diffractive wakeup call can be defined by the information of the time-of-flight array. The information from this array is bundled into 576 segments covering the full central barrel. Each of these segments covers an area of approximately  $30 \times 50 \text{ cm}^2$  and delivers one bit per beam bunch crossing depending on whether a track has been seen within the segment. A logic trigger unit collects the 576 bits and can set multiplicity conditions and topological constraints. In addition, the information of the V0A and V0C detectors is available at this level hence the required gap width can be defined.

The output of this trigger unit is fast enough to reach the ALICE central trigger processor well before the time limit for L0 decision.

The information of the zero degree calorimeter can be used in the high-level trigger HLT to identify different diffractive event classes. Reactions of the type  $pp \rightarrow ppX$  do not carry a signal in the zero degree calorimeters. Here, X denotes a centrally produced diffractive state. Events of the type  $pp \rightarrow pN^*X$  are characterized by a signal in one of the two calorimeters whereas events  $pp \rightarrow N^*N^*X$  carry a signal in both calorimeters.

## 2 Signatures of Pomeron

The geometry of the ALICE experiment is suited for measuring a centrally produced diffractive state with a rapidity gap on either side. Such a topology results from double Pomeron exchange with subsequent hadronization of the central state. It is expected that the secondaries from these Pomeron-Pomeron fusion events show markedly different characteristics as compared to secondaries from inelastic minimum bias events.

First, it is expected that the production cross section of glueball states in Pomeron fusion is larger as compared to inelastic minimum bias events. It will therefore be interesting to study the resonances produced in the central region when two rapidity gaps are required[4].

Second, the slope  $\alpha'$  of the Pomeron trajectory is rather small:  $\alpha' \sim 0.25 \text{ GeV}^{-2}$  in DL fit and  $\alpha' \sim 0.1 \text{ GeV}^{-2}$  in vector meson production at HERA[5]. These values of  $\alpha'$  in conjunction with the small t-slope ( $< 1 \text{ GeV}^{-2}$ ) of the triple Pomeron vertex indicate that the mean transverse momentum  $k_t$  in the Pomeron wave function is relatively large  $\alpha' \sim 1/k_t^2$ , most probably  $k_t > 1 \text{ GeV}$ . The transverse momenta of secondaries produced in Pomeron-Pomeron interactions are of the order of this  $k_t$ . Thus the mean transverse momenta of secondaries produced in Pomeron-Pomeron fusion is expected to be larger as compared to inelastic minimum bias events.

Third, the large  $k_t$  described above corresponds to a large effective temperature. A suppression of strange quark production is not expected. Hence the K/ $\pi$  ratio is expected to be enhanced in Pomeron-Pomeron fusion as compared to inelastic minimum bias events. Similarly, the  $\eta/\pi$  and  $\eta'/\pi$  ratios are expected to be enhanced due to the hidden strangeness content and due to the gluon components in the Fock states of  $\eta, \eta'$ .

## 3 Signatures of Odderon

The Odderon was first postulated in 1973 and is represented by color singlet exchange with negative C-parity[6]. Due to its negative C-parity, Odderon exchange can lead to differences between particle-particle and particle-antiparticle scattering. In QCD, the Odderon can be a three gluon object in a symmetric color state. Due to the third gluon involved in the exchange, a suppression by the coupling  $\alpha_s$  is expected as compared to the two gluon Pomeron exchange. However, finding experimental signatures of the Odderon exchange has so far turned out to be extremely difficult[7]. A continued non-observation of Odderon signatures would put considerable doubt on the formulation of high energy scattering by gluon exchange[8]. The best evidence so far for Odderon exchange was established as a difference between the differential cross sections for elastic  $pp$  and  $p\bar{p}$  scattering at  $\sqrt{s} = 53 \text{ GeV}$  at the CERN ISR. The  $pp$  cross section displays a dip at  $t = -1.3 \text{ GeV}^2$  whereas the  $p\bar{p}$  cross section levels off. Such a behaviour is typical for negative C-exchange and cannot be due to mesonic Reggeons only.

Signatures of Odderon exchanges can be looked for in exclusive reactions where the Odderon (besides the Photon) is the only possible exchange. Diffractively produced C-even states such as pseudoscalar or tensor mesons can result from Photon-Photon, Photon-Odderon and Odderon-Odderon exchange. Any excess measured beyond the well understood Photon-Photon contribution would indicate an Odderon contribution.

Diffractively produced C-odd states such as vector mesons  $\phi$ ,  $J/\psi$ ,  $\Upsilon$  can result from Photon-Pomeron or Odderon-Pomeron exchange. Any excess beyond the Photon contribution would be indication of Odderon exchange.

Estimates of cross section for diffractively produced  $J/\psi$  in pp collisions at LHC energies were first given by Schäfer et al[9]. More refined calculations by Bzdak et al result in a t-integrated photon contribution of  $\frac{d\sigma}{dy}|_{y=0} \sim 15$  nb and a t-integrated Odderon contribution of  $\frac{d\sigma}{dy}|_{y=0} \sim 1$  nb[10]. These two numbers carry large uncertainties, the upper and lower limit of these numbers vary by about an order of magnitude. This cross section is, however, at a level where in  $10^6$  s of ALICE data taking the  $J/\psi$  can be measured in its  $e^+e^-$  decay channel at a level of 4% statistical uncertainty. Due to the different t-dependence, the Photon and Odderon contribution result in different transverse momentum distribution  $p_T$  of the  $J/\psi$ . A careful transverse momentum analysis of the  $J/\psi$  might therefore allow to disentangle the Odderon contribution.

If the diffractively produced final state is not an eigenstate of C-parity, then interference effects between Photon-Pomeron and Photon-Odderon amplitudes can be analyzed[11]. Charge asymmetry in pion or kaon pairs is thought to be sizable[12, 13]. From the transverse momenta of the two particles in the pairs, the vectors of sum and difference can be calculated. The sum is C-even whereas the difference is C-odd. The opening angle  $\alpha$  between sum and difference vector behaves as  $\alpha \rightarrow \alpha + \pi$  under C-parity, hence a Fourier analysis of the  $\alpha$ -distribution will allow to quantify the C-odd contribution.

## 4 Photoproduction of heavy quarks

Diffractive reactions involve scattering on small-x gluons in the proton. The number density of gluons at given x increases with  $Q^2$ , as described by the DGLAP evolution. Here,  $Q^2$  and x denote the kinematical parameters used in deep inelastic ep scattering. The transverse gluon density at a given  $Q^2$  increases with decreasing x as described by the BFKL evolution equation. At some density, gluons will overlap and hence reinteract. In this regime, the gluon density saturates and the linear DGLAP and BFKL equation reach their range of applicability. A saturation scale  $Q_s(x)$  is defined which represents the breakdown of the linear regime. Nonlinear effects become visible for  $Q < Q_s(x)$ .

Diffractive heavy quark photoproduction represents an interesting probe to look for gluon saturation effects at LHC. The inclusive cross section for  $Q\bar{Q}$  photoproduction can be calculated within the dipole formalism. In this approach, the photon fluctuates into a  $Q\bar{Q}$  excitation which interacts with the proton as a color dipole. The dipole cross section  $\sigma(x,r)$  depends on x as well as on the transverse distance r of the  $Q\bar{Q}$  pair. A study of inclusive heavy quark photoproduction in pp collisions at LHC energy has been carried out[14]. These studies arrive at differential cross sections for open charm photoproduction of  $\frac{d\sigma}{dy}|_{y=0} \sim 1.3$   $\mu\text{b}$  within the collinear pQCD approach as compared to  $\frac{d\sigma}{dy}|_{y=0} \sim 0.4$   $\mu\text{b}$  within the color glass condensate (CGC). The cross sections are such that open charm photoproduction seems measurable with good statistical significance. The corresponding numbers for the cross section for bottom photoproduction are  $\frac{d\sigma}{dy}|_{y=0} \sim 20$  nb and 10 nb, respectively.

Diffraction photoproduction is characterized by two rapidity gaps in the final state. In the dipole formalism described above, the two gluons of the color dipole interaction are in color singlet state. Diffractive heavy quark photoproduction cross sections in pp, pPb and PbPb collisions at LHC have been studied[15]. The cross sections for diffractive charm photoproduction are  $\frac{d\sigma}{dy}|_{y=0} \sim 6$  nb in pp,  $\frac{d\sigma}{dy}|_{y=0} \sim 9$   $\mu$ b in pPb and  $\frac{d\sigma}{dy}|_{y=0} \sim 11$  mb in PbPb collisions. The corresponding numbers for diffractive bottom photoproduction are  $\frac{d\sigma}{dy}|_{y=0} \sim 0.014$  nb in pp,  $\frac{d\sigma}{dy}|_{y=0} \sim 0.016$   $\mu$ b in pPb and  $\frac{d\sigma}{dy}|_{y=0} \sim 0.02$  mb in PbPb collisions.

Heavy quarks with two rapidity gaps in the final state can, however, also be produced by central exclusive production, i.e. two Pomeron fusion. The two production mechanisms have a different  $t$ -dependence. A careful analysis of the transverse momentum  $p_T$  of the  $Q\bar{Q}$  pair might therefore allow to disentangle the two contributions.

### Acknowledgments

This work was supported in part by German BMBF under project 06HD197D.

## References

- [1] ALICE Collaboration et al 2004, J.Phys. G: Nucl. Part. Phys. **30** 1517-1763
- [2] ALICE Collaboration et al 2006, J.Phys. G: Nucl. Part. Phys. **32** 1295-2040
- [3] R.Arnaldi et al, Nucl. Instr. and Meth. A **564** (2006) 235
- [4] F.Close,A.Kirk,G.Schuler, Phys.Lett. B **477** (2000) 13
- [5] A.Donnachie,P.Landshoff, Phys.Lett. B**595** (2004) 393
- [6] L.Lukaszuk,B.Nicolescu, Lett. Nuovo Cim. **8** (1973) 406
- [7] C.Ewerz, Proceedings XII Rencontres de Blois (2005) 377
- [8] S.Donnachie,G.Dosch,P.V.Landshoff,O.Nachtmann, Pomeron physics and QCD, Cambridge University Press (2002) 297
- [9] A.Schäfer,L.Mankiewicz,O.Nachtmann, Phys.Lett. B **272** (1991) 419
- [10] A.Bzdak,L.Motyka,L.Szymanowski,J.R.Cudell, Phys.Rev. D **75** (2007) 094023
- [11] S.J.Brodsky,J.Rathsman,C.Merino, Phys.Lett. B **461** (1999) 114
- [12] P.Hägler,B.Pire,L.Szymanowski,O.V.Teryaev, Phys.Lett. B **535** (2002) 117
- [13] I.F.Ginzburg,I.P.Ivanov,N.N.Nikolaev, Eur.Phys.J. C**5** (2003) 02
- [14] V.P.Goncalves,M.V.Machado, Phys.Rev.D **71** (2005) 014025
- [15] V.P.Goncalves,M.V.Machado, Phys.Rev.D **75** (2007) 031502